

# Microwave-Assisted Nanocellulose Synthesis from Seaweed: TiO<sub>2</sub>/ZnO-Modified Membrane for Seawater Treatment

Anwar Said <sup>1,\*</sup>, Maulina Maulina <sup>2</sup>, Faizal Mustapa <sup>3,\*</sup> 

<sup>1</sup> Department of Fishery Products Technology, Faculty of Fisheries and Marine Science, Universitas Muhammadiyah Kendari, Kendari 93127, Southeast Sulawesi, Indonesia

<sup>2</sup> Department of English Language Education, Universitas Muhammadiyah Kendari, Kendari 93127, Southeast Sulawesi, Indonesia

<sup>3</sup> Department of Marine Sciences, Institut Teknologi dan Bisnis Muhammadiyah Kolaka, Kolaka 93511, Southeast Sulawesi, Indonesia

\* Correspondence: [anwar.said@umkendari.ac.id](mailto:anwar.said@umkendari.ac.id) (A.S.), [ichalgowamekong28@gmail.com](mailto:ichalgowamekong28@gmail.com) (F.M.);

Received: 28.09.2024; Accepted: 15.07.2025; Published: 25.11.2025

**Abstract:** This study explores the sustainable synthesis of nanocellulose (NC) from seaweed biomass via microwave-assisted processing, followed by modification with TiO<sub>2</sub> and ZnO to enhance membrane properties for water purification applications. The unique attributes of cellulose, such as biodegradability and high mechanical strength, coupled with the photocatalytic and antibacterial properties of TiO<sub>2</sub> and ZnO, present a compelling case for the development of multifunctional membranes. Characterization techniques, including Fourier transform infrared (FTIR) spectroscopy, X-ray diffraction (XRD), and scanning electron microscopy (SEM), were employed to assess the physicochemical properties and structural integrity of the synthesized membranes. Results indicated that the NC/TiO<sub>2</sub>/ZnO membrane exhibited a significantly higher flux (169.85 L/m<sup>2</sup> h) and enhanced salt rejection (82.0%) compared to the control NC membrane (141.54 L/m<sup>2</sup>.h and 80.0%, respectively). These findings underscore the potential of integrating renewable biomass with advanced materials to create effective, environmentally friendly solutions for addressing water treatment challenges. The enhanced flux and salt rejection efficiency achieved by the NC/TiO<sub>2</sub>/ZnO membrane suggest its promising applicability in addressing water treatment challenges and promoting sustainable material development in industrial settings.

**Keywords:** membrane; microwave; nanocellulose; seaweed; TiO<sub>2</sub>/ZnO.

© 2025 by the authors. This article is an open-access article distributed under the terms and conditions of the Creative Commons Attribution (CC BY) license (<https://creativecommons.org/licenses/by/4.0/>), which permits unrestricted use, distribution, and reproduction in any medium, provided the original work is properly cited. The authors retain copyright of their work, and no permission is required from the authors or the publisher to reuse or distribute this article, as long as proper attribution is given to the original source.

## 1. Introduction

Cellulose ranks among the most abundant natural biopolymers on the planet. Its versatility has led to broad use across multiple sectors, including papermaking, food packaging, pharmaceuticals, and the fabrication of eco-friendly composite material[1–3]. Owing to its remarkable features—including high mechanical strength and stiffness, extensive surface area, favorable aspect ratio, light weight, cost-effectiveness, recyclability, and biodegradability—cellulose holds great potential for a wide range of industrial applications [1,4,5]. The environmental benefits of recyclable, biodegradable cellulose are further driving the market's

future growth across various green applications [6,7]. The growing interest in cellulose nanomaterials is driven by increasing environmental concerns, which require developing biodegradable materials with broad applications and extraordinary properties [1,3,7].

Over the past few decades, considerable research attention has been directed toward isolating cellulose nanomaterials from biomass, with nanocellulose emerging as one of the most widely explored derivatives [8,9]. Nanocellulose (NC), an environmentally friendly material, has attracted significant attention due to its remarkable properties, including high mechanical strength, biocompatibility, and biodegradability [1,7,10–12]. NC is produced from abundant biomass resources, and its use is growing in various applications, including composite materials [13], filtration membranes [14,15], and catalyst supports [8,16]. One emerging approach for NC production is through sustainable synthesis using renewable bioresources [13,15]. Seaweed biomass has been identified as an attractive biomass source for NC production due to its abundance, rapid growth, and high fiber content [17–19]. Seaweed has advantages over terrestrial biomass sources, such as not competing with food production and not requiring large land areas for cultivation. The process of converting seaweed biomass into NC not only reduces the dependence on terrestrial biomass sources but also supports the concept of circular economy and environmental sustainability. Various research reports have highlighted the need to develop efficient techniques for NC production for multiple applications [11,13–15].

Microwave-based synthesis methods have emerged as more efficient and environmentally friendly approaches for processing biomass [20,21]. This technology uses microwave energy to accelerate hydrolysis, producing NCs with shorter reaction times and lower energy consumption than conventional methods. This microwave-based method can also reduce hazardous chemicals, making it more sustainable for NC production. In this study, NCs were synthesized without undergoing a dewaxing process. Microwave radiation was used as an alternative energy source due to its ability to generate heat rapidly [19]. NCs were extracted from seaweed. In addition, we present the first successful experiment to isolate nanocellulose crystals from this marine biomass using a microwave-assisted method with alkalization, bleaching, and acid hydrolysis, as reported by Singh.

TiO<sub>2</sub> and ZnO have been widely used in material development as membrane modification materials due to their photocatalytic and antibacterial properties [22,23]. Combining NC with TiO<sub>2</sub>/ZnO nanoparticles can produce membranes with superior properties, including high mechanical strength, photocatalytic activity, and enhanced filtration performance [24,25]. These modified membranes are highly promising for water purification, gas separation, and industrial wastewater treatment.

This study aims to develop a sustainable NC synthesis method using microwave heating from seaweed biomass and to modify the resulting NCs with TiO<sub>2</sub>/ZnO to create multifunctional membranes. Characterization of these composite materials will provide deeper insight into the physicochemical properties of the synthesized NC and how TiO<sub>2</sub>/ZnO modification improves its performance in various applications. By combining renewable biomass, environmentally friendly technologies, and advanced functional materials, this study aims to develop green materials that support global sustainability goals. The physicochemical properties and structural changes of the NC membrane produced from TiO<sub>2</sub>/ZnO-modified seaweed were systematically tested through chemical functional group analysis (FTIR), crystallinity (XRD), and morphology studies (SEM). This study presents a novel approach to nanocellulose synthesis, utilizing a microwave-assisted method to extract nanocellulose from

seaweed biomass. This technique offers several advantages over conventional methods, including reduced processing time, lower energy consumption, and minimized use of hazardous chemicals, contributing to a more sustainable and efficient nanocellulose production process.

## 2. Materials and Methods

### 2.1. Materials.

Seaweed was obtained from Bungin Village, South Konawe Regency, Southeast Sulawesi. Sodium hydroxide (NaOH), Hydrochloric acid (HCl, for analysis 37%), ethanol (EtOH, for analysis 100 vol.%), acetone (CH<sub>3</sub>COCH<sub>3</sub>, for analysis 100 vol.%), Hydrogen peroxide (H<sub>2</sub>O<sub>2</sub>, for analysis 32 vol.%) was purchased from Merck Indonesia, titanium (IV) oxide (TiO<sub>2</sub>), zinc oxide (ZnO), and Polyethylene Glycol (PEG) from Sigma-Aldrich.

### 2.2. Instruments.

Fourier transform infrared (FTIR) spectra were recorded with a Shimadzu IR Prestige-21 spectrometer in 600–4000 cm<sup>-1</sup>. X-ray diffraction (XRD) was performed with a Bruker D2-phaser X-ray diffractometer for Cu K $\alpha$  radiation ( $\lambda = 1.5406 \text{ \AA}$ ) in the 10–90° range. Scanning electron microscopy (SEM) images were recorded using a Hitachi SU8220 (HITACHI, Tokyo, Japan) with a tungsten filament as the electron source operated at 18 kV.

### 2.3. Synthesis of nanocellulose by seaweed biomass.

The seaweed was initially rinsed with deionized water to eliminate impurities and subsequently dried in an oven at 80 °C for 24 hours. It was then milled into fine particles smaller than 100  $\mu\text{m}$ . A 50 g seaweed powder sample was pre-treated for alkalization treatment with 2.5 M NaOH under microwave irradiation for 50 min at 200 W. The obtained slurry was cooled to room temperature and filtered under vacuum using Whatman No. 3 filter paper. The extract was repeatedly rinsed with hot deionized water until a neutral pH was achieved. For all subsequent experimental procedures, deionized water was employed. The material was then oven-dried at 55 °C overnight. Next, it was bleached using 32% H<sub>2</sub>O<sub>2</sub> for 6 h with constant stirring at 55°C to remove lignin. The resulting sample was washed repeatedly with hot deionized water and kept at room temperature overnight. The bleached sample was further hydrolyzed in 1.5 M HCl in a microwave for 30 min at 400 W. After the mixture reached boiling, it was left overnight and washed several times with deionized water to a pH of 6~7. The obtained NC samples were dried for further characterization. This method is a modification of Singh's research [19]. The isolation procedure scheme is given in Figure 1.

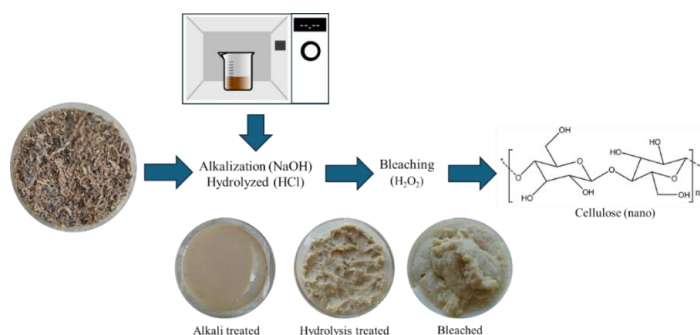


**Figure 1.** Synthesis of nanocellulose from seaweed biomass by microwave method.

#### 2.4. Synthesis of TiO<sub>2</sub>/ZnO.

TiO<sub>2</sub> and ZnO were each weighed at 0.5 g and added to 9 mL of ethanol. The resulting solution was poured into a glass bottle and stirred for 30 min. Then, the mixture was exposed to microwave irradiation at 400 W for 30 min. The obtained solid was filtered and repeatedly washed with deionized water. The resulting powder was then oven-dried at 150 °C for 5 hours prior to further characterization.

#### 2.5. Synthesis of TiO<sub>2</sub>/ZnO modified nanocellulose.

The manufacture of TiO<sub>2</sub>/ZnO-modified nanocellulose membranes was carried out using the Blending method. The blending method was carried out by weighing 0.5 grams of TiO<sub>2</sub>/ZnO. 17 mL of acetone was added to TiO<sub>2</sub>/ZnO and stirred without heating. NC and polyethylene glycol were added 2 and 1 g, respectively, while heated at 130°C with stirring until homogeneous. The membrane was molded using a mold and soaked in distilled water at room temperature for 15 minutes. Furthermore, the membrane was dried at 50°C for 30 minutes and left at room temperature. A comparison membrane, the NC membrane without TiO<sub>2</sub>/ZnO, is manufactured using the same procedure.

#### 2.6. Membrane testing and performance evaluation.

The performance of both the NC (control) and NC/TiO<sub>2</sub>/ZnO membranes was assessed by evaluating their water flux and salt rejection efficiency. The water flux was measured by passing a known volume of water (Q) through the membrane under a constant pressure over a fixed period (t). The effective surface area (A) of the membrane was calculated using its radius (r). For each membrane, the flux value was recorded and compared, as presented in Table 1. The experiment was conducted at room temperature, and the flux measurement for each membrane type was repeated three times to ensure reliability.

To evaluate salt rejection efficiency, a 35% synthetic seawater solution was passed through each membrane under controlled pressure. The concentration of salt in the permeate (C<sub>p</sub>) was measured using a conductivity meter, along with the salt rejection percentage. The flux values and salt rejection efficiencies of the NC/TiO<sub>2</sub>/ZnO and control membranes were statistically analyzed to assess the impact of TiO<sub>2</sub> and ZnO modification on membrane performance. The experimental results were interpreted by comparing the control and modified membranes, evaluating the influence of TiO<sub>2</sub> and ZnO on hydrophilicity, porosity, and overall filtration performance. The collected data were validated by comparing them with previously published research to ensure consistency and accuracy. This comprehensive methodology ensured a robust evaluation of the potential of the NC/TiO<sub>2</sub>/ZnO membrane for enhanced water treatment applications.

### 3. Result and Discussion

#### 3.1. Characterization of membrane.

The FTIR spectrum in Figure 2a shows the spectrum representing different samples, namely NC (a), TiO<sub>2</sub>/ZnO (b), NC membrane (c), and NC/TiO<sub>2</sub>/ZnO membrane (d). Analysis of each spectrum provides information about its functional groups. The FTIR spectrum of NC shows a characteristic band at a wave number of around 3442.94 cm<sup>-1</sup>, indicating the presence of hydroxyl group (O-H) vibrations, and a band around 2918.30 cm<sup>-1</sup> associated with C-H

vibrations of methyl or methylene groups in the cellulose structure. The absorption peak of the benzene ring framework appears at  $1462.04\text{ cm}^{-1}$ , which is most likely derived from the deformation vibration of C-H or C-O-H bonds in the cellulose structure. The band at  $1653\text{ cm}^{-1}$  is characteristic of cellulose, which is probably associated with vibrations of adsorbed water or hydrogen bonds in the polysaccharide chain. However, under certain conditions, it can also be caused by C=O (carbonyl) groups, particularly during cellulose degradation or oxidative modification[25]. Carbonyl groups are not commonly found in pure cellulose but can appear when cellulose is oxidized or when impurities, for example, from chemical reaction by-products, are present. In addition, there is a band around  $1000\text{--}1200\text{ cm}^{-1}$  related to vibrations of the C-O bond in the cellulose structure. This ether group is formed by the  $\beta$ -1,4-glycosidic bond connecting the glucose units in the polymer, as indicated by the peak at  $1029\text{ cm}^{-1}$  [26].

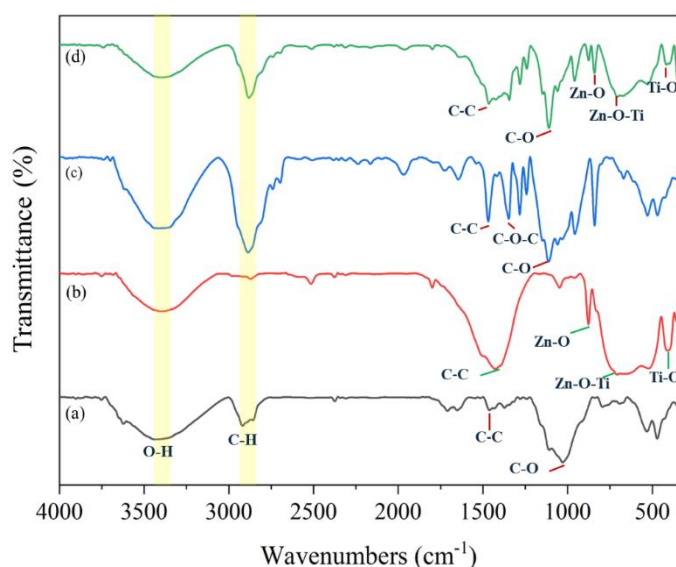


**Figure 2.** FT-IR spectrum of (a) NC; (b)  $\text{TiO}_2/\text{ZnO}$ ; (c) membrane NC; (d) membrane NC/ $\text{TiO}_2/\text{ZnO}$ .

In the FTIR spectrum (b), a new band appears at around  $500\text{--}700\text{ cm}^{-1}$ , related to the vibration of Ti-O and Zn-O, confirming the presence of  $\text{TiO}_2$  and ZnO in the material.  $\text{TiO}_2$  and ZnO often have hydroxyl groups attached to their surfaces due to forming bonds with water or environmental humidity [25]. Ethanol can leave -OH groups from solvent molecules that are adsorbed or weakly bound to the surface of  $\text{TiO}_2/\text{ZnO}$ . This causes the appearance of the -OH peak at around  $3390\text{ cm}^{-1}$ . The peak at  $1427.3\text{ cm}^{-1}$  is likely due to the C-C stretching vibration, which may arise from residual ethanol as a solvent or from organic contamination during the synthesis process. The nanocellulose membrane shows a spectral shift, with a more intense band at  $3388.93\text{ cm}^{-1}$  (O-H group), indicating stronger intermolecular hydrogen bonding. The C-O band is also more clearly seen in the  $1000\text{--}1200\text{ cm}^{-1}$  region, reinforcing that the main component is cellulose. The broad band around  $2881.65\text{ cm}^{-1}$  is the C-H vibration of methyl or methylene groups in the cellulose and PEG structures. The band at  $1348.24\text{ cm}^{-1}$  shows the typical C-O-C vibration of PEG. In the FTIR spectrum (d), the combination of nanocellulose with  $\text{TiO}_2$  and ZnO causes the appearance of bands around  $500\text{--}700\text{ cm}^{-1}$  representing the vibration of Zn-O and Ti-O [22], like spectrum (b). In addition, the presence of bands around  $1000\text{--}1200\text{ cm}^{-1}$  indicates the C-O bond of nanocellulose, and some weak bands around  $1600\text{ cm}^{-1}$  indicate the interaction between nanocellulose and metal oxide particles. Overall, these spectra show significant differences between samples, especially in the wavenumber regions associated with O-H, C-H, C-O, and metal oxide (Ti-O, Zn-O) groups,

confirming the presence of chemical interactions and structural changes between NC, TiO<sub>2</sub>, and ZnO during membrane formation.

The XRD results confirmed the crystallinity and structure of the regenerated NCs, as shown in Figure 3(a). It shows the peaks of NCs around  $2\theta = 18.85^\circ$ ,  $23.05^\circ$ , and  $26.5^\circ$ , which indicate the (110), (200), and (004) planes, respectively, in Figure 3(a). These peaks are characteristic of the cellulose II structure and the typical bands of cellulose nanoparticles, as reported elsewhere [26]. The structural changes might be due to the alkaline treatment for MNC, which causes the reduction of crystallinity. The size of the regenerated NCs can be observed at  $2\theta = 23.05^\circ$ . Based on the research of Li *et al.* [26], the XRD pattern of ZnO corresponds well to the hexagonal wurtzite phase (JCPDS No. 36-1451). In contrast, TiO<sub>2</sub> alone can be assigned to the anatase phase (JCPDS No. 65-5714) [27]. For the TiO<sub>2</sub>/ZnO composite, diffraction peaks associated with both anatase TiO<sub>2</sub> and wurtzite ZnO are evident, indicating that the synthesized material consists of these two components. In the diffraction pattern shown in Figure 3(c), the prominent peaks of ZnO are located at around  $2\theta = 31.5^\circ$ ,  $34.3^\circ$ , and  $36.11^\circ$ , which belong to the (100), (002), and (101) planes, respectively. The main peaks of tetragonal anatase TiO<sub>2</sub> at  $2\theta$  values of  $25.5^\circ$ ,  $40.0^\circ$ ,  $48.0^\circ$ ,  $54.2^\circ$ , and  $62.4^\circ$ , corresponding to the atomic planes (101), (004), (200), (105), and (211), are shown in Figure 3(b). TiO<sub>2</sub>/ZnO material shows the essential peaks of TiO<sub>2</sub> at around  $25.5^\circ$ ,  $38.20^\circ$ ,  $48.32^\circ$ , and  $54.69^\circ$ . In addition, the crystallite size of TiO<sub>2</sub>/ZnO is about 34.4 nm, as calculated based on Debye-Scherrer's equation. The NC/TiO<sub>2</sub>/ZnO membrane is shown in Figure 3(d), and the diffraction peaks of NC and TiO<sub>2</sub>/ZnO show their characteristic peaks. The study showed the success of synthesizing TiO<sub>2</sub>/ZnO, NC, and NC/TiO<sub>2</sub>/ZnO membranes.

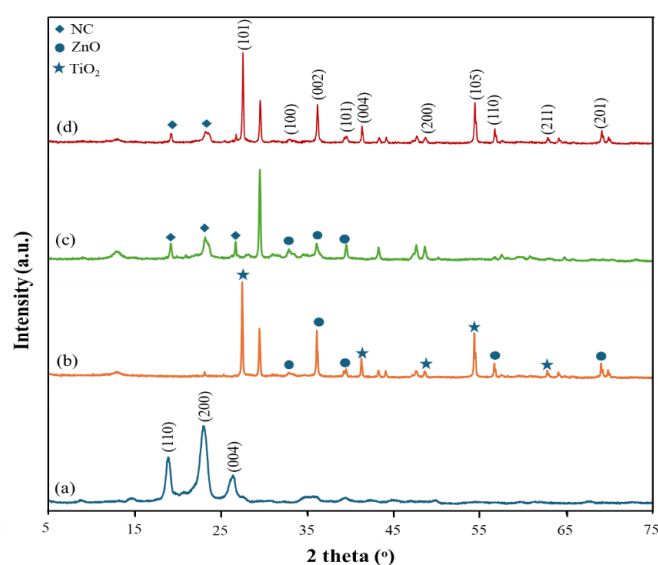


**Figure 3.** X-ray diffraction pattern of the membrane (a) NC; (b) TiO<sub>2</sub>/ZnO; (c) membrane NC/ZnO; (d) membrane NC/TiO<sub>2</sub>/ZnO.

A morphological investigation was conducted on TiO<sub>2</sub>/ZnO using an SEM analysis, as shown in Figure 4a. The morphological image of TiO<sub>2</sub>/ZnO at a 10  $\mu\text{m}$  scale showed a relatively uniform particle distribution, indicating the formation of aggregate nanoparticles. Based on the study, the morphology of ZnO was distributed in a non-uniform rod shape and irregular shape on the surface [28]. In addition, TiO<sub>2</sub> had a uniform size distribution of small rod grains with a width and length. The particles appeared dense and showed a rough surface texture, which could benefit applications requiring high surface area, such as photocatalysis or sensing. The appearance of TiO<sub>2</sub>/ZnO showed a high degree of aggregation with a grain-like

morphology and the growth of ZnO into a smooth rectangular shape, which was in good agreement with the XRD results. TiO<sub>2</sub> grains were seen to grow in addition to the aggregated rod grains. These aggregates likely increased surface reactivity due to their larger surface area-to-volume ratio. The nanoscale roughness observed here is typical of mixed-oxide materials and indicates that the TiO<sub>2</sub> and ZnO components are well integrated.

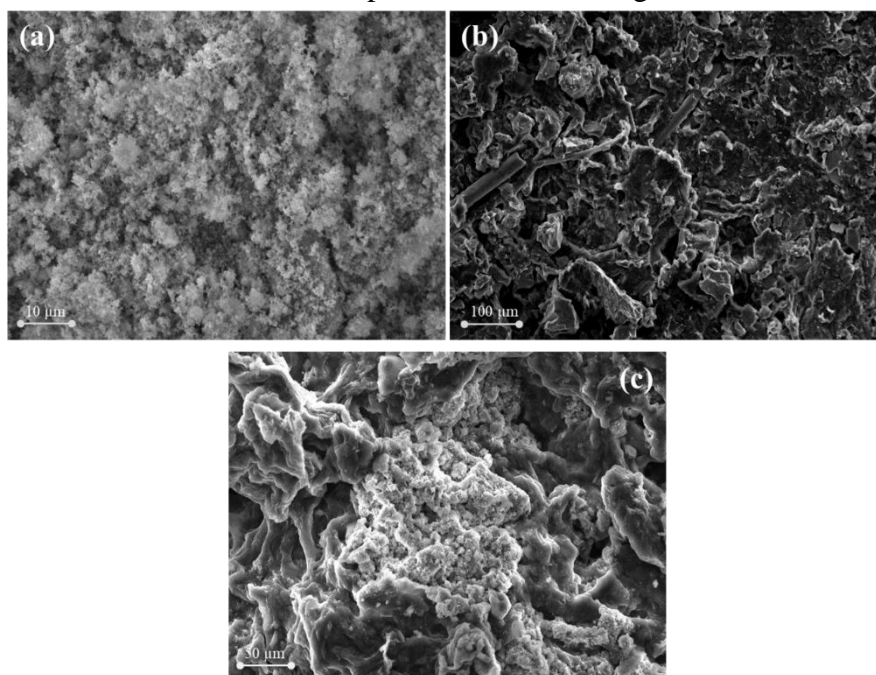


**Figure 4.** SEM image of (a) TiO<sub>2</sub>/ZnO; (b) membrane NC; (c) membrane NC/TiO<sub>2</sub>/ZnO.

The NC membrane exhibits a fibrous and porous structure at the 100 μm scale, as shown in Figure 4b. This fibrillar network is characteristic of cellulose-based materials, providing high mechanical strength and flexibility. The open, interconnected pores are likely responsible for the membrane's permeability and filtration properties. The NC membrane presents a porous architecture with a rough surface. [29,30]. This porosity is essential for applications such as filtration or as a supporting matrix for active particles. The fibrous texture indicates the presence of well-formed NC fibrils, which are crucial to mechanical reinforcement and stability in composite materials. The membranes containing NC and TiO<sub>2</sub>/ZnO exhibited hybrid morphology at a 50 μm scale, as shown in Figure 4c. Nanoscale TiO<sub>2</sub>/ZnO particles were observed as aggregates distributed in the fibrous structure of NC membranes. This created a rough, complex surface with a more pronounced texture and possibly enhanced functional properties, due to the combination of the NC fibrous network and TiO<sub>2</sub>/ZnO photocatalytic/antimicrobial properties. [24,28]. The membranes showed good integration of TiO<sub>2</sub>/ZnO materials within the NC matrix, thereby enhancing their functional properties. The composite structure could benefit from the mechanical robustness of NC and the reactive surface properties of TiO<sub>2</sub>/ZnO. This combination could be highly advantageous for applications in water purification, where photocatalytic filtration and degradation of contaminants are desired.

### 3.2. Membrane performance.

Based on the data presented in Table 1, the experimental results indicate that the NC/TiO<sub>2</sub>/ZnO membrane achieved a flux value of 169.85 L/m<sup>2</sup> h, which is significantly higher than the 141.54 L/m<sup>2</sup> h observed for the control NC membrane, suggesting that the

incorporation of TiO<sub>2</sub> and ZnO into the membrane matrix effectively enhances permeability and filtration efficiency. These findings align with the research by [31,32], which demonstrated that adding TiO<sub>2</sub> particles to membranes improves hydrophilicity and pore-size distribution, thereby increasing water flux and filtration efficiency. The integration of inorganic materials, such as TiO<sub>2</sub>, into membrane structures has been shown to elevate performance in desalination and water filtration processes, making them more effective for industrial applications. The flux calculations in Figure 5 further validate this enhancement, as the NC/TiO<sub>2</sub>/ZnO membrane consistently showed higher flux than the control NC membrane, reinforcing the conclusion that modification with TiO<sub>2</sub> and ZnO significantly improves membrane permeability. Collectively, these results confirm that membrane modification with inorganic materials such as TiO<sub>2</sub> holds considerable potential to enhance filtration performance, indicating substantial applicability in advanced water treatment processes.

**Table 1.** The result of identifying the calculation value of the membrane flux.

Treatments	Q (Liter)	radius (m)	$\pi$	t (hour)	A (m <sup>2</sup> )	Flux (L/m <sup>2</sup> h)
NC (Control)	0.2	0.03	3.14	0.5	0.002826	141.5428
NC/TiO <sub>2</sub> /ZnO	0.24	0.03	3.14	0.5	0.002826	169.8514

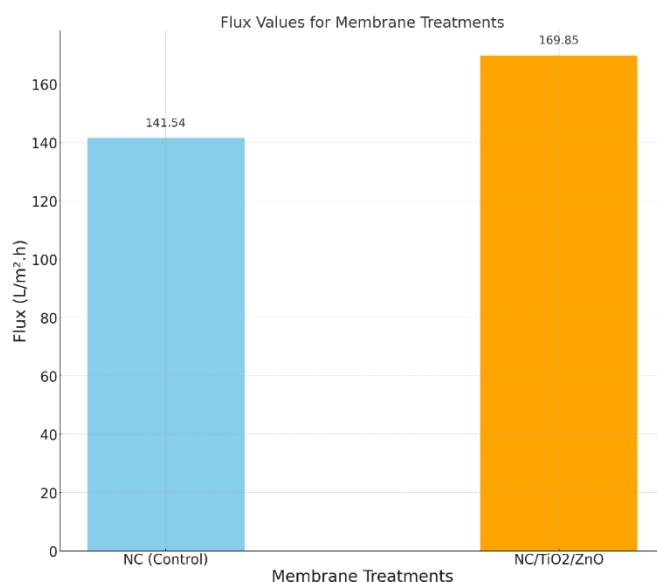


**Figure 5.** Evaluation of the flux measurements for each membrane.

The experimental results demonstrate that the NC/TiO<sub>2</sub>/ZnO membrane exhibits higher salt rejection efficiency than the control membrane, as shown in Table 2. The control membrane recorded a salt rejection rate of 80.0%, whereas the NC/TiO<sub>2</sub>/ZnO membrane showed an increased efficiency of 82.0%. This difference indicates that membrane modification with NC/TiO<sub>2</sub>/ZnO materials enhances its effectiveness in filtering salt from seawater. The improved efficiency is likely due to the hydrophilic properties and increased porosity imparted by the addition of TiO<sub>2</sub> and ZnO, which significantly enhance the membrane's ability to filter salt particles. These findings highlight the potential of the NC/TiO<sub>2</sub>/ZnO membrane for desalination applications, demonstrating superior performance compared to the control membrane.

**Table 2.** Assessment of salt rejection values from membrane testing results.

Treatments	Cp (permeate concentration %)	C0 (seawater concentration %)	Salt rejection (%)
NC (Control)	7	35	80
NC/TiO <sub>2</sub> /ZnO	6.3	35	82

## 4. Conclusions

The successful synthesis of nanocellulose from seaweed biomass via microwave-assisted processing demonstrates the viability of renewable resources for producing high-performance materials. The subsequent modification of nanocellulose with TiO<sub>2</sub> and ZnO significantly enhanced the mechanical and filtration properties of the resulting membranes. Characterization techniques confirmed the structural integrity and functional interactions within the composite materials. The NC/TiO<sub>2</sub>/ZnO membrane not only achieved superior water flux and salt rejection but also demonstrated potential for application in advanced water purification processes. This study highlights the importance of developing sustainable materials that align with environmental goals while addressing critical challenges in water treatment. The integration of biopolymers with photocatalytic nanoparticles paves the way for innovative solutions that support the principles of a circular economy.

## Author Contributions

Conceptualization, A.A.; methodology, A.A.; formal analysis, F.M.; validation, F.M.; writing—original draft preparation, M.M. All authors have read and agreed to the published version of the manuscript.

## Institutional Review Board Statement

Not applicable.

## Informed Consent Statement

Not applicable.

## Data Availability Statement

Data supporting the findings of this study are available upon reasonable request from the corresponding author.

## Funding

We acknowledge the financial support from the Ministry of Education, Culture, Research, and Technology of the Republic of Indonesia under the Fundamental Research award grant no. 111/E5/PG.02.00.PL/2024 and 642/LL9/PK.00.PG/2024.

## Acknowledgments

We acknowledge the support of the Universitas Muhammadiyah Kendari for the laboratory facilities.

## Conflicts of Interest

The authors declare no conflict of interest.

## References

1. Ansari, M.M.; Heo, Y.; Do, K.; Ghosh, M.; Son, Y.-O. Nanocellulose derived from agricultural biowaste by-products—Sustainable synthesis, biocompatibility, biomedical applications, and future perspectives: A review. *Carbohydr. Polym. Technol. Appl.* **2024**, *8*, 100529, <https://doi.org/10.1016/j.carpta.2024.100529>.
2. Xu, Y.; Wu, Z.; Li, A.; Chen, N.; Rao, J.; Zeng, Q. Nanocellulose Composite Films in Food Packaging Materials: A Review. *Polymers* **2024**, *16*, 423, <https://doi.org/10.3390/polym16030423>.
3. Li, J.; Zhang, F.; Zhong, Y.; Zhao, Y.; Gao, P.; Tian, F.; Zhang, X.; Zhou, R.; Cullen, P.J. Emerging Food Packaging Applications of Cellulose Nanocomposites: A Review. *Polymers* **2022**, *14*, 4025, <https://doi.org/10.3390/polym14194025>.
4. Emenike, E.C.; Iwuzor, K.O.; Saliu, O.D.; Ramontja, J.; Adeniyi, A.G. Advances in the extraction, classification, modification, emerging and advanced applications of crystalline cellulose: A review. *Carbohydr. Polym. Technol. Appl.* **2023**, *6*, 100337, <https://doi.org/10.1016/j.carpta.2023.100337>.
5. Zaaba, N.F.; Jaafar, M.; Ismail, H. Tensile and morphological properties of nanocrystalline cellulose and nanofibrillated cellulose reinforced PLA bionanocomposites: A review. *Polym. Eng. Sci.* **2021**, *61*, 22–38, <https://doi.org/10.1002/pen.25560>.
6. Chen, Z.; Aziz, T.; Sun, H.; Ullah, A.; Ali, A.; Cheng, L.; Ullah, R.; Khan, F. U. Advances and applications of cellulose bio-composites in biodegradable materials. *J. Polym. Environ.* **2023**, *31*, 2273–2284, <https://doi.org/10.1007/s10924-022-02561-8>.
7. Aziz, T.; Li, W.; Zhu, J.; Chen, B. Developing multifunctional cellulose derivatives for environmental and biomedical applications: Insights into modification processes and advanced material properties. *Int. J. Biol. Macromol.* **2024**, *278*, 134695, <https://doi.org/10.1016/j.ijbiomac.2024.134695>.
8. Marakana, P.G.; Dey, A.; Saini, B. Isolation of nanocellulose from lignocellulosic biomass: Synthesis, characterization, modification, and potential applications. *J. Environ. Chem. Eng.* **2021**, *9*, 106606, <https://doi.org/10.1016/j.jece.2021.106606>.
9. Cheng, Z.; Li, J.; Wang, B.; Zeng, J.; Xu, J.; Zhu, S.; Duan, C.; Chen, K. Comparative study on properties of nanocellulose derived from sustainable biomass resources. *Cellulose* **2022**, *29*, 7083–7098, <https://doi.org/10.1007/s10570-022-04717-0>.
10. Zhang, H.-C.; Yu, C.-N.; Li, X.-Z.; Wang, L.-F.; Huang, J.; Tong, J.; Lin, Y.; Min, Y.; Liang, Y. Recent Developments of Nanocellulose and Its Applications in Polymeric Composites. *ES Food Agrofor.* **2022**, *9*, 1–14, <https://doi.org/10.30919/esfaf768>.
11. Patil, T.V.; Patel, D.K.; Dutta, S.D.; Ganguly, K.; Santra, T.S.; Lim, K.-T. Nanocellulose, a versatile platform: From the delivery of active molecules to tissue engineering applications. *Bioact. Mater.* **2022**, *9*, 566–589, <https://doi.org/10.1016/j.bioactmat.2021.07.006>.
12. Khalid, M.Y.; Al Rashid, A.; Arif, Z.U.; Ahmed, W.; Arshad, H. Recent advances in nanocellulose-based different biomaterials: types, properties, and emerging applications. *J. Mater. Res. Technol.* **2021**, *14*, 2601–2623, <https://doi.org/10.1016/j.jmrt.2021.07.128>.
13. Gupta, G.K.; Shukla, P. Lignocellulosic Biomass for the Synthesis of Nanocellulose and Its Eco-Friendly Advanced Applications. *Front. Chem.* **2020**, *8*, 601256, <https://doi.org/10.3389/fchem.2020.601256>.
14. Yuan, B.; Li, L.; Murugadoss, V.; Vupputuri, S.; Wang, J.; Alikhani, N.; Guo, Z. Nanocellulose-based Composite Materials for Wastewater Treatment and Waste-oil Remediation. *ES Food Agrofor.* **2020**, *1*, 41–52, <https://doi.org/10.30919/esfaf0004>.
15. Jaffar, S.S.; Saallah, S.; Misson, M.; Siddiquee, S.; Roslan, J.; Saalah, S.; Lenggoro, W. Recent Development and Environmental Applications of Nanocellulose-Based Membranes. *Membranes* **2022**, *12*, 287, <https://doi.org/10.3390/membranes12030287>.
16. Maiuolo, L.; Algieri, V.; Olivito, F.; Tallarida, M.A.; Costanzo, P.; Jiritano, A.; De Nino, A. Chronicle of Nanocelluloses (NCs) for Catalytic Applications: Key Advances. *Catalysts* **2021**, *11*, 96, <https://doi.org/10.3390/catal11010096>.
17. Zhou, Y.; Liu, L.; Li, M.; Hu, C. Algal biomass valorisation to high-value chemicals and bioproducts: Recent advances, opportunities and challenges. *Bioresour. Technol.* **2022**, *344*, 126371, <https://doi.org/10.1016/j.biortech.2021.126371>.
18. Mouga, T.; Fernandes, I.B. The Red Seaweed Giant Gelidium (*Gelidium corneum*) for New Bio-Based Materials in a Circular Economy Framework. *Earth* **2022**, *3*, 788–813, <https://doi.org/10.3390/earth3030045>.

19. Singh, S.; Gaikwad, K.K.; Park, S.-I.; Lee, Y.S. Microwave-assisted step reduced extraction of seaweed (*Gelidium aceroso*) cellulose nanocrystals. *Int. J. Biol. Macromol.* **2017**, *99*, 506-510, <https://doi.org/10.1016/j.ijbiomac.2017.03.004>.
20. Sidana, A.; Yadav, S.K. Recent developments in lignocellulosic biomass pretreatment with a focus on eco-friendly, non-conventional methods. *J. Clean. Prod.* **2022**, *335*, 130286, <https://doi.org/10.1016/j.jclepro.2021.130286>.
21. Adeola, A.O.; Duarte, M.P.; Naccache, R. Microwave-assisted synthesis of carbon-based nanomaterials from biobased resources for water treatment applications: emerging trends and prospects. *Front. Carbon* **2023**, *2*, 1220021, <https://doi.org/10.3389/frcarb.2023.1220021>.
22. Soria, R.B.; Zhu, J.; Gonza, I.; Van der Bruggen, B.; Luis, P. Effect of (TiO<sub>2</sub>: ZnO) ratio on the anti-fouling properties of bio-inspired nanofiltration membranes. *Sep. Purif. Technol.* **2020**, *251*, 117280, <https://doi.org/10.1016/j.seppur.2020.117280>.
23. Menazea, A.A.; Awwad, N.S. Antibacterial activity of TiO<sub>2</sub> doped ZnO composite synthesized via laser ablation route for antimicrobial application. *J. Mater. Res. Technol.* **2020**, *9*, 9434-9441, <https://doi.org/10.1016/j.jmrt.2020.05.103>.
24. Sosa, S.M.; Huertas, R.; Pereira, V.J. Combination of Zinc Oxide Photocatalysis with Membrane Filtration for Surface Water Disinfection. *Membranes* **2023**, *13*, 56, <https://doi.org/10.3390/membranes13010056>.
25. Li, C.; Liu, Q.; Shu, S.; Xie, Y.; Zhao, Y.; Chen, B.; Dong, W. Preparation and characterization of regenerated cellulose/TiO<sub>2</sub>/ZnO nanocomposites and its photocatalytic activity. *Mater. Lett.* **2014**, *117*, 234-236, <https://doi.org/10.1016/j.matlet.2013.12.009>.
26. Bhutiya, P.L.; Misra, N.; Rasheed, M.A.; Hasan, S.Z. Silver Nanoparticles Deposited Algal Nanofibrous Cellulose Sheet for Antibacterial Activity. *BioNanoScience* **2020**, *10*, 23-33, <https://doi.org/10.1007/s12668-019-00690-4>.
27. Li, J.; Yan, L.; Wang, Y.; Kang, Y.; Wang, C.; Yang, S. Fabrication of TiO<sub>2</sub>/ZnO composite nanofibers with enhanced photocatalytic activity. *J. Mater. Sci.: Mater. Electron.* **2016**, *27*, 7834-7838, <https://doi.org/10.1007/s10854-016-4773-1>.
28. Abd El-Kader, M.F.H.; Elabbasy, M.T.; Adeboye, A.A.; Zeariya, M.G.M.; Menazea, A.A. Morphological, structural and antibacterial behavior of eco-friendly of ZnO/TiO<sub>2</sub> nanocomposite synthesized via *Hibiscus rosa-sinensis* extract. *J. Mater. Res. Technol.* **2021**, *15*, 2213-2220, <https://doi.org/10.1016/j.jmrt.2021.09.048>.
29. Aguilar-Sanchez, A.; Jalvo, B.; Mautner, A.; Nameer, S.; Pöhler, T.; Tammelin, T.; Mathew, A.P. Waterborne nanocellulose coatings for improving the antifouling and antibacterial properties of polyethersulfone membranes. *J. Membr. Sci.* **2021**, *620*, 118842, <https://doi.org/10.1016/j.memsci.2020.118842>.
30. Mautner, A.; Bismarck, A. Bacterial nanocellulose papers with high porosity for optimized permeance and rejection of nm-sized pollutants. *Carbohydr. Polym.* **2021**, *251*, 117130, <https://doi.org/10.1016/j.carbpol.2020.117130>.
31. Mustapa, F.; Nurdin, M.; Muzakkar, M.Z.; Idris, M. Mesoporous CA/PEG Membrane-Modified TiO<sub>2</sub> Nanoparticles with Improved Desalination Performance. *Biointerface Res. Appl. Chem.* **2024**, *14*, 29, <https://doi.org/10.33263/BRIAC142.029>.
32. Shishov, A.; Gagarionova, S.; Bulatov, A. Deep eutectic mixture membrane-based microextraction: HPLC-FLD determination of phenols in smoked food samples. *Food Chem.* **2020**, *314*, 126097, <https://doi.org/10.1016/j.foodchem.2019.126097>.

## Publisher's Note & Disclaimer

The statements, opinions, and data presented in this publication are solely those of the individual author(s) and contributor(s) and do not necessarily reflect the views of the publisher and/or the editor(s). The publisher and/or the editor(s) disclaim any responsibility for the accuracy, completeness, or reliability of the content. Neither the publisher nor the editor(s) assume any legal liability for any errors, omissions, or consequences arising from the use of the information presented in this publication. Furthermore, the publisher and/or the editor(s) disclaim any liability for any injury, damage, or loss to persons or property that may result from the use of any ideas, methods, instructions, or products mentioned in the content. Readers are encouraged to independently verify any information before relying on it, and the publisher assumes no responsibility for any consequences arising from the use of materials contained in this publication.